RSC Pharmaceutics

ROYAL SOCIETY OF CHEMISTRY

COMMUNICATION

View Article Online
View Journal

Cite this: DOI: 10.1039/d5pm00203f

Received 28th July 2025,
Accepted 28th October 2025

DOI: 10.1039/d5pm00203f

rsc.li/RSCPharma

Systemic drug delivery in pigs using biodegradable microneedle patches

Katherine A. Miranda-Muñoz,[a] Tsungcheng Tsai,[b] Jacy L. Riddle,[b] Ke He,[c] Lee Blaney,[c] Jeremy G. Powell[b] and Jorge Almodovar *[c]

Transdermal microneedle systems offer a minimally invasive strategy for systemic drug delivery in veterinary medicine. In this study, biodegradable microneedle patches composed of polyvinyl alcohol, collagen, and chitosan were evaluated in pigs for the delivery of two model compounds, fluorescein isothiocyanate–dextran (FITC-dextran, 4 kDa) and flunixin meglumine (FLU). Patches were applied to the ear and neck to assess the influence of anatomical site on systemic absorption. FITC-dextran delivered *via* a single 50 mg patch on the neck achieved approximately 1.2–1.4-fold higher plasma concentrations than oral administration and ear-applied patches, demonstrating enhanced uptake from vascularized regions. FLU patches applied to the ear produced detectable plasma levels up to 72 h post-application, with a maximum concentration of ~1.9 μg L^{-1} at 24–48 h, indicating sustained systemic exposure and reinforcing the potential for long-acting therapy. No adverse tissue responses were observed at application sites, highlighting the safety and tolerability of the patches. Overall, these findings emphasize the importance of anatomical site selection, physicochemical properties, and biocompatibility in optimizing microneedle-mediated transdermal drug delivery for veterinary applications.

Introduction

Effective pain management in livestock is challenged by limitations in current delivery methods and restrictions on analgesic use in food-producing animals.[1–4] Injectable and oral drugs require repeated handling and may result in variable systemic exposure.[5,6] These challenges highlight the urgent need for welfare-friendly, minimally invasive drug delivery systems that reduce animal discomfort while maintaining precision dosing and therapeutic efficacy. In this regard, microneedle patches have emerged as a promising option, offering needle-free, stress-free, transdermal delivery capable of circumventing first-pass metabolism and improving drug absorption.[7,8] However, systemic drug uptake remains inconsistent, especially for compounds with low aqueous solubility or limited permeability.[9]

Our group previously developed a biodegradable microneedle platform composed of polyvinyl alcohol (PVA), collagen (COL), and chitosan (CHI) for delivery of meloxicam in piglets.[10] While this system demonstrated successful microneedle dissolution and local drug release, systemic meloxicam absorption was limited, likely due to the low solubility and permeability of this compound (Class IV, BCS).[9] These results raised key questions about whether systemic uptake was primarily affected by anatomical factors, microneedle performance, or the inherent physicochemical properties of the drug.

To better understand the performance of biodegradable microneedle patches, this study focused on evaluating the effect of anatomical application site on uptake of two compounds with greater solubility and permeability than meloxicam, namely fluorescein isothiocyanate-dextran (FITC-dextran) and flunixin meglumine (FLU). FITC-dextran is a hydrophilic fluorescent tracer widely used as a model drug in transdermal delivery research. The high solubility and molecular stability of FITC-dextran are ideal for evaluating microneedle performance, skin penetration, and delivery system performance.[11,12] FITC-dextran enables fluorescence-based quantitation of absorption kinetics and provides a reliable means to distinguish whether bioavailability limitations arise from anatomical site differences or delivery system performance.[13,14]

FLU is a potent, non-narcotic, nonsteroidal anti-inflammatory drug (NSAID) widely used in veterinary medicine to manage pain, inflammation, and fever in both food-producing and companion animals.[15,16] The meglumine salt form of FLU provides high aqueous solubility and favorable permeability, leading to rapid systemic absorption when administered *via* traditional parenteral routes.[17,18] Given its widespread clinical use, well-established pharmacokinetics, and regulatory importance (*e.g.*, defined withdrawal times for meat-producing animals), FLU was

[a]*Department of Biomedical Engineering, College of Engineering, University of Arkansas, Fayetteville, AR 72701, USA*
[b]*Department of Animal Sciences, University of Arkansas, B110 Agriculture, Food and Life Sciences Building, Fayetteville, AR 72701, USA*
[c]*Department of Chemical, Biochemical, and Environmental Engineering, University of Maryland Baltimore County, 1000 Hilltop Circle, Baltimore, MD 21250, USA. E-mail: almodova@umbc.edu; Tel: +1 410-455-3400*

identified as a valuable model compound for evaluating microneedle-based transdermal drug delivery systems.

In this study, microneedle patches loaded with either FITC-dextran or FLU were applied to the ear and neck of piglets to evaluate how anatomical site and drug properties influence systemic uptake. These regions were selected for their distinct vascularization, dermal thickness, and lymphatic drainage. Plasma samples collected over time were analyzed to compare absorption profiles and identify site-specific differences in drug delivery performance. The aggregate results offer new insights for optimization of microneedle-based transdermal systems in veterinary medicine.

Methodology

Microneedle patch fabrication

Microneedle patches were fabricated following a modified version of the protocol described in Miranda-Muñoz *et al.*[10] Briefly, the patches were produced using a 25 mm × 25 mm polydimethylsiloxane (PDMS) mold with 625 pyramidal microneedles. Each microneedle had a base width of 400 μm, a height of 800 μm, and a pitch of 700 μm (Fig. 1A). The polymeric formulation consisted of variable ratios of PVA and COL; FITC-dextran and FLU were incorporated at a dose of 50 mg per patch. The microneedle layer was cast in the PDMS mold and allowed to dry under controlled conditions to ensure uniform drug distribution (Fig. 1B). Once the microneedle layer was set, a secondary layer composed of PVA–CHI was applied to enhance adhesion and mechanical integrity. Then, the patches were sterilized using ethylene oxide gas. Fourier transform infrared spectroscopy and morphological analyses confirmed that ethylene oxide sterilization did not alter drug stability or patch composition.[10] Macroscopic and scanning electron microscopy (SEM) imaging were performed to assess microneedle patch morphology, including needle geometry, uniformity, and structural integrity. In particular, an ultrahigh resolution field emission SEM (FEI Nova Nanolab 200) was used to analyze the shape, size, and surface features of PVA–COL–CHI microneedle patches loaded with FITC-dextran or FLU. Gold coating was not required, as the samples exhibited adequate conductivity under the selected imaging conditions.

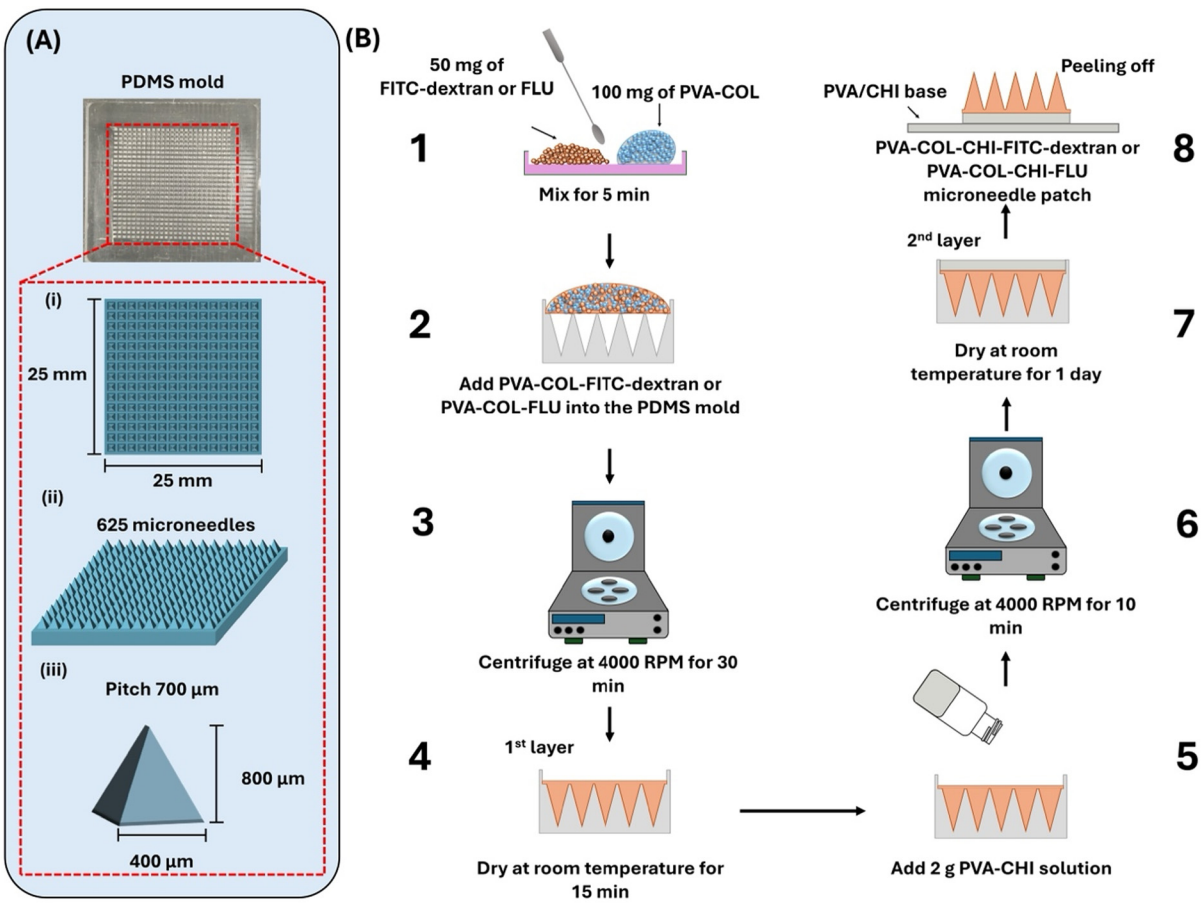

Fig. 1 Microneedle patch design and fabrication process. (A) Schematic view of the PDMS mold and microneedle patch with structural information: (i) top view and dimensions; (ii) slanted view showing 625 microneedles; and (iii) side view of a single microneedle and its dimensions. (B) Schematic representation of the fabrication process for PVA–COL–CHI–FITC-dextran or PVA–COL–CHI–FLU microneedle patches. The process includes mixing PVA–COL with FITC-dextran or FLU, casting the solution in a PDMS mold, centrifuging, drying, and layering with PVA–CHI to form a structured microneedle patch.

In vivo study

All animal procedures were performed in accordance with the Guidelines for Care and Use of Laboratory Animals of University of Arkansas Division of Agriculture Swine Research Farm and approved by the Animal Ethics Committee of the Institutional Animal Care and Use Committee (IACUC approval number: 23066). A total of 16 piglets from two litters were randomly assigned to six treatment groups: (1) negative controls (n = 2); (2) oral FITC-dextran administration at 10 mg kg^{-1} of piglet body weight (n = 2); (3) a single 50 mg FITC-dextran microneedle patch on the right ear (n = 3); (4) a single 50 mg FITC-dextran patch on each ear (n = 3); (5) a single 50 mg FITC-dextran microneedle patch on the neck (n = 3); and (6) a single 50 mg FLU microneedle patch on the right ear (n = 3). Groups 3 and 4 were designed to assess the influence of total dose on systemic uptake while controlling for anatomical site. Groups 3 and 5 were included to inform the role of anatomical location and local vascularization on systemic uptake, and Groups 3 and 6 were designed to address the role of drug solubility and permeability on systemic uptake; both of these comparisons controlled for total drug dose.

Prior to patch application, the skin at the ear and neck sites was cleaned and sterilized using alcohol wipes. The patches were secured using adhesive medical dressing to prevent premature detachment. At predetermined times (*i.e.*, 0, 4, 8, 24, 48, 72, 96 h), blood samples were collected *via* jugular venipuncture using S-Monovette® needles (22-gauge, 1 in) and deposited in S-Monovette® EDTA K3E blood collection tubes (SARSTEDT Inc., Newton, NC). In one piglet, the patch was removed after 24 h to visually observe microneedle degradation. The whole blood was centrifuged at 1500*g*, and plasma was isolated for analysis of drug concentrations. Results were presented as mean ± standard deviation, but we focused on descriptive analysis due to the limited number of animals per group (n = 2–3). Formal statistical comparisons between groups were not performed, as the study was designed as a pilot exploration.

Drug analysis

FITC-dextran (from Sigma-Aldrich, St Louis, MO) concentrations in plasma were directly determined by fluorescence spectrophotometry (Biotek Synergy HTX, Agilent Technologies Inc., Santa Clara, CA) using excitation and emission wavelengths of 480 nm and 520 nm, respectively.

FLU, 5-hydroxyflunixin (5H-FLU; metabolite), and FLU-d_3 (internal standard) were purchased from Sigma-Aldrich (St Louis, MO). Anhydrous magnesium sulfate ($MgSO_4$), sodium chloride (NaCl), ammonium acetate (NH_4Ac), and LC-MS grade water, methanol, and acetonitrile were obtained from Fisher Scientific (Waltham, MA). Stock and working solutions were prepared in methanol, and the final calibration standards were prepared in 50% methanol with 10 mM NH_4Ac.

The plasma concentrations of FLU and 5H-FLU were measured *via* QuEChERS extraction followed by liquid chromatography with triple quadrupole tandem mass spectrometry (LC-MS/MS); the protocols were adapted from a previous method.[19] Briefly, a 100 µL aliquot of plasma was transferred to a 15 mL centrifuge tube, diluted with 1.9 mL deionized water, and vortexed for 30 s. Then, 2 mL acetonitrile, 1 g $MgSO_4$, and 0.4 g NaCl were added to enable salting-out phenomena, causing FLU to partition into the acetonitrile layer; to homogenize the mixture, 30 s vortex steps were included after addition of acetonitrile and the salts. After 10 min of centrifugation at 6000*g*, 1.5 mL of the acetonitrile layer was collected, evaporated to dryness with nitrogen gas, reconstituted in 0.25 mL methanol containing 20 µg L^{-1} FLU-d_3, and diluted with 0.25 mL of 10 mM NH_4Ac solution. The reconstituted extracts were analyzed by LC-MS/MS.

FLU, 5H-FLU, and FLU-d_3 were measured with an Agilent 1290 Infinity LC coupled to a 6470 triple quadrupole MS/MS (Agilent; Santa Clara, CA). The injection volume was 5 µL, and the analytes were separated along a Waters XBridge C18 column (2.1 × 150 mm, 2.5 µm) with a guard column (2.1 × 10 mm, 3.0 µm) containing the same material. The column compartment was maintained at 40 °C. The mobile phase was comprised of (A) LC-MS water with 10 mM NH_4Ac (pH 6.9) and (B) LC-MS methanol with 10 mM NH_4Ac. Isocratic elution was applied with 40% A and 60% B at a flow rate of 0.2 mL min^{-1}, and the run time was 7 min. The MS/MS was operated in positive electrospray ionization mode. The capillary voltage was 3500 V. The drying and sheath gases were maintained at 300 °C and 7 L min^{-1}, and the nebulizer pressure was set to 45 psi. Other settings and method performance metrics are summarized in Table 1.

Table 1 LC-MS/MS operational parameters and method performance metrics

Compound	MW[a]	Ion transitions[b]	CE[c]	FV[d]	Ratio[e]	RT[f]	LOQ[g]	LOD[h]	MQL[i]	MDL[j]	R^2	IS[k]
FLU	296.2	**297.1 → 279.0**	22	90	0.20	5.83	0.10	0.03	0.50	0.15	0.999	FLU-d_3
		297.1 → 263.9	33									
5H-FLU	312.2	**312.9 → 295.0**	23	90	0.30	4.71	1.00	0.30	5.00	1.50	0.994	FLU-d_3
		312.9 → 279.9	34									
FLU-d_3	299.3	**300.1 → 282.0**	22	90	0.20	5.82	—	—	—		—	—
		300.1 → 263.9	33									

[a] Molecular weight (MW; Da). [b] The first ion transition was used for quantitation, and the *second ion transition* was used for confirmation. [c] Collision energy (CE; V). [d] Fragmentor voltage (FV; V). [e] The response of the confirmation ion divided by the response of the quantitation ion. [f] Retention time (RT; min). [g] Limit of quantitation (LOQ; µg L^{-1}), calculated using the signal-to-noise ratio (>10), the method blank, and the weighted calibration curve. [h] Limit of detection (LOD; µg L^{-1}), calculated as 3/10 of the LOQ. [i] Method quantitation limit (MQL; µg L^{-1}), calculated for 100 µL plasma samples. [j] Method detection limit (MDL; µg L^{-1}), calculated as 3/10 of the MQL. [k] Internal standard (IS).

FLU recovery from each plasma sample was evaluated through standard additions. In particular, 50 μL of a solution containing 100 μg L^{-1} FLU and 100 μg L^{-1} 5H-FLU was spiked into a separate 100 μL plasma aliquot and diluted with 1.85 mL of deionized water. This sample underwent the same extraction and analysis protocols described above. FLU recovery ranged from 85.8 to 93.0% for individual samples, and the average recovery was 89.7 ± 2.7%. The FLU recovery efficiency was applied to correct the concentrations measured in the QuEChERS extracts to ensure accurate reporting of FLU concentrations in the plasma samples.[19]

Results and discussion

Microneedle patches were fabricated using PVA–COL–CHI blends that incorporated either FITC-dextran or FLU. The macroscopic and SEM images in Fig. 2 revealed well-defined, uniformly distributed microneedles for both formulations. No structural defects, such as tip deformation or fusion, were observed, confirming the high reproducibility and fidelity of the fabrication process. Notably, the side faces of the FITC-dextran microneedles were flatter than the FLU-loaded microneedles, which displayed a subtle curvature. This variation in geometry may result from differences in polymer viscosity, drug loading, or mold filling dynamics and could potentially influence mechanical performance and drug delivery. Overall, the results suggest uniform drug loading and compatibility with the polymer matrix, supporting the suitability of the microneedle patches for *in vivo* evaluations.

Fig. 3 summarizes the *in vivo* evaluation of PVA–COL–CHI microneedle patches loaded with FITC-dextran or FLU by highlighting the experimental design, anatomical site comparisons, and systemic drug absorption profiles. The study design and application sites are reported in Fig. 3A, which shows that patches were placed on the ear and neck to investigate anatomical effects on drug delivery. The schematic also outlines the different experimental groups, including negative controls, oral FITC-dextran administration, and various microneedle patch configurations. To further illustrate the *in vivo* methodology used to assess pharmacokinetic outcomes, the experimental procedure for microneedle patch application is shown in Fig. 3D, and a representative image of the microneedle patch after removal from the skin is provided in Fig. 3E.

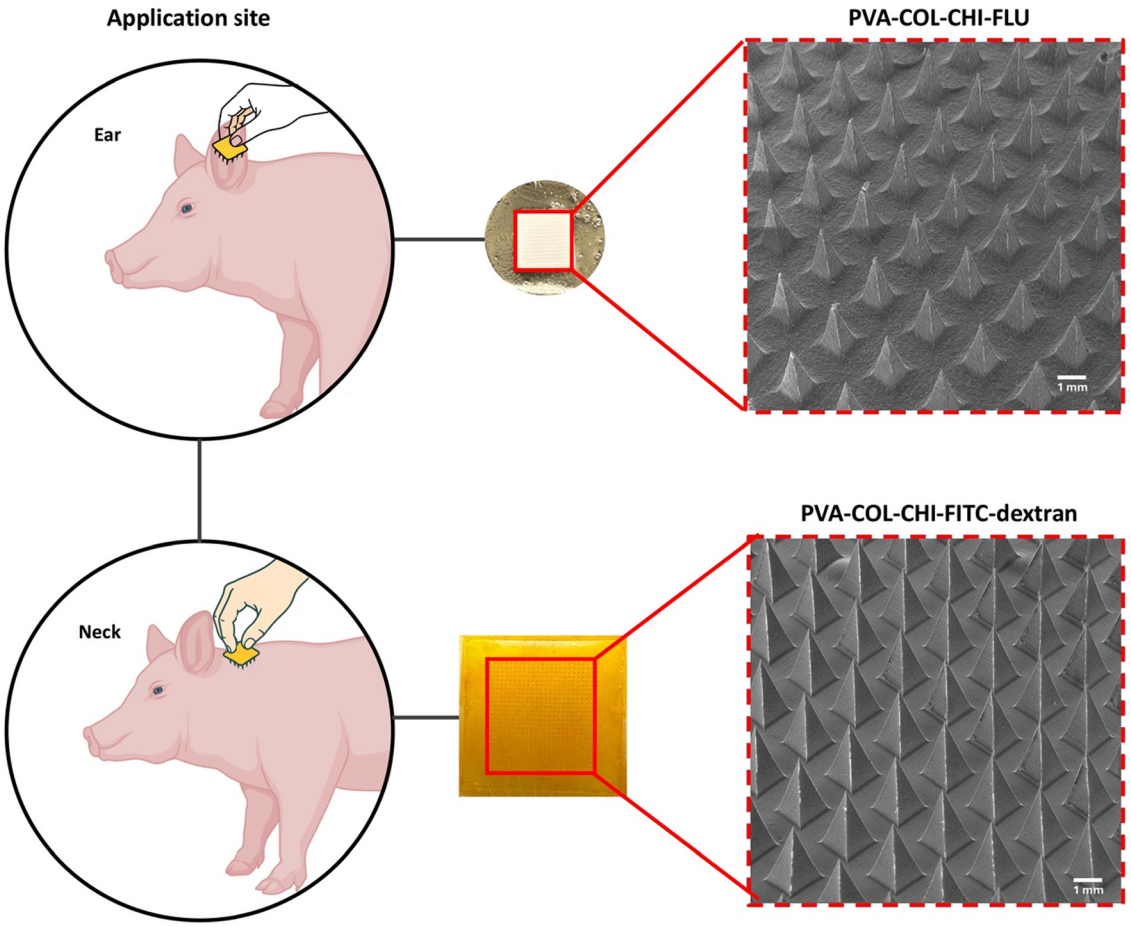

Fig. 2 Application sites and morphological analysis of microneedle patches. Macroscopic (center) and SEM (right) images of PVA–COL–CHI patches loaded with FLU or FITC-dextran highlight the consistent microneedle geometry.

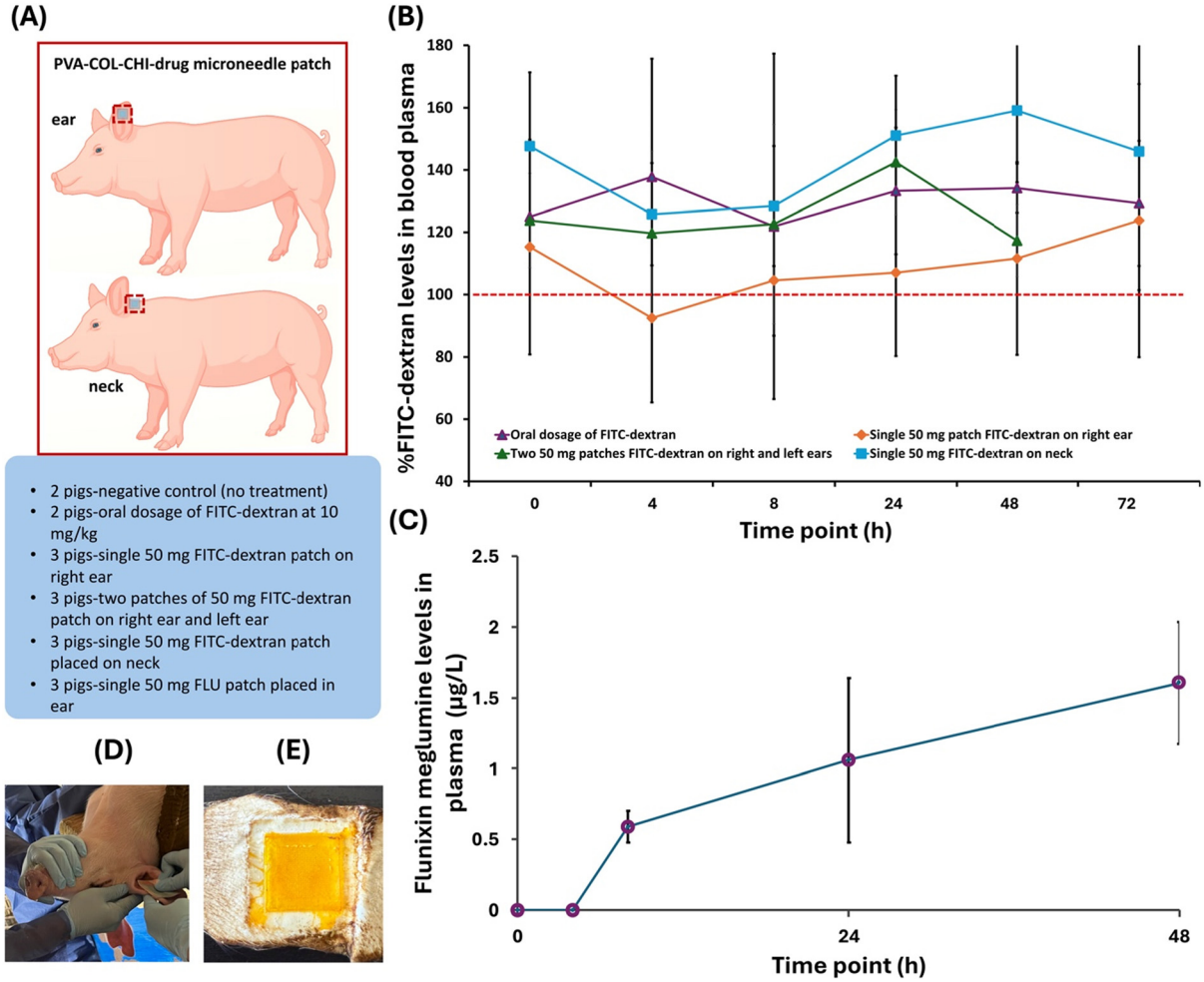

Fig. 3 *In vivo* evaluation of FITC-dextran and FLU delivery using microneedle patches. (A) Experimental design. (B) Plasma FITC-dextran levels following oral delivery (10 mg kg^{-1}), single (ear/neck) and dual (both ears) 50 mg patches. (C) Plasma FLU levels after applying a single 50 mg patch on the ear. (D) Representative photo of patch application. (E) Microneedle patch 24 h post-application. Study groups included negative control, oral FITC-dextran, and five patch configurations for FITC-dextran and FLU.

The FITC-dextran levels in plasma after application of microneedle patches revealed notable differences in systemic uptake depending on delivery mechanism and anatomical site (Fig. 3B). After 24 h, the single 50 mg patch applied to the neck produced the highest plasma concentrations of FITC-dextran (145 μg L^{-1}), exceeding oral administration (120 μg L^{-1}) and the ear-applied patches (95 μg L^{-1} for a single patch; 120 μg L^{-1} for two patches). For context, the piglets had an average body weight of approximately 3.9 kg (4.2 kg, 3.7 kg, and 3.8 kg), and the oral dose was administered at 10 mg per kg body weight, resulting in a total dose of approximately 39 mg per pig. In comparison, each microneedle patch contained a fixed dose of 50 mg of FITC-dextran, independent of body weight. The elevated FTIC-dextran concentrations from the neck patch were maintained at most post-application times, whereas moderate and relatively stable systemic levels were observed for oral administration. FITC-dextran digestive absorption efficiency depends on the level of intestinal development and the integrity of the tight junction protein.[20–22] While the exact fraction of FITC-dextran systemically absorbed cannot be determined without bioavailability studies, this comparison underscores differences in delivery efficiency and highlights the potential of site-specific patch placement to enhance systemic uptake. These results were considered promising but interpreted as preliminary and hypothesis-generating given the limited sample size (n = 2–3 per group), which precluded formal statistical comparisons.

The findings reported in Fig. 3B highlight the critical role of anatomical site selection in microneedle-mediated transdermal delivery. The better absorption of FITC-dextran observed for the neck application was presumably due to the greater vascularization and thinner skin, which facilitate more efficient drug transport into circulation. In contrast, the lower uptake of FITC-dextran from ear-applied patches may stem from limited blood flow and structural barriers in piglet ears. Interestingly, the plasma concentrations of FITC-dextran in

piglets with one patch on each ear (*i.e.*, two patches) were only 10–40% greater than for piglets with one patch on the right ear (*i.e.*, one patch) (Fig. 3B). These outcomes confirm that drug absorption was governed more by site-specific physiological properties than by the dose loaded to microneedle patches.

The fluctuations in plasma concentrations of FITC-dextran over time (Fig. 3B) indicated that transdermal absorption was a dynamic process influenced by multiple factors. Metabolic clearance likely played a role in the observed variability, as systemic circulation and enzymatic degradation contribute to elimination.[23–25] Circulatory factors, such as differences in blood flow, may have also influenced drug uptake and distribution.[26–28] Moreover, the rate of microneedle dissolution could have varied in the skin at each site, leading to variable drug release kinetics and systemic absorption.[29,30] In previous work, we used a ballistic gel to evaluate the *in vitro* release and diffusion of fluorescein from microneedle patches.[10] The diffusion of fluorescein followed a controlled released behavior, unlike the FITC-dextran release profile observed in this *in vivo* study. While ballistic gel tests provided a simulated model of microneedle dissolution, those experiments could not fully replicate *in vivo* conditions, which involve interactions with biological tissues, differences in hydration levels and enzymatic activity, and other factors that impact microneedle dissolution. This outcome underscores the need for future *in vivo* studies to accurately characterize how microneedle dissolution rates influence drug release kinetics and overall systemic absorption.

Microneedle patches loaded with 50 mg FLU were applied to the ear in three piglets to assess whether systemic delivery would be improved for a more water-soluble NSAID. Data were only collected for two animals due to the loss of one subject during the study. Plasma concentrations of FLU peaked at 24–48 h post-application, with a maximum concentration of 1.9 μg L^{-1} (Fig. 3C). Although FLU exhibits greater aqueous solubility and membrane permeability than FITC-dextran, the systemic levels achieved *via* microneedle-mediated transdermal delivery were substantially lower than those associated with therapeutic efficacy. For example, intramuscular administration of FLU at 2.2 mg kg^{-1} in mature pigs resulted in peak plasma concentrations ranging from 2749 to 6004 μg L^{-1}.[31] In contrast, a recent study in pre-wean piglets using a 3.3 mg kg^{-1} transdermal dose, applied as a pour-on liquid, reported a maximum concentration of 31.5 μg L^{-1} FLU at 24 h post-application.[32] While the observed plasma concentrations were lower for the 50 mg FLU loaded microneedle patch, the data aligned with the expected pharmacokinetic profile for transdermal delivery, namely slower absorption and lower bioavailability. The delayed time to maximum plasma concentration (24–48 h) reflects the inherently slower absorption kinetics of transdermal routes and suggests that our microneedle-based system may achieve relatively higher plasma concentrations than other administration techniques at later times.

The above results indicate that drug solubility and permeability did not overcome the anatomical limitations of patch application to the ear. The slow systemic uptake and subtherapeutic concentrations of FLU observed in Fig. 3C support the hypothesis that local physiological characteristics, such as low vascular perfusion and increased dermal thickness, play a central role in limiting drug absorption from ear-applied patches. These results also motivate further studies to assess alternative application sites, such as the neck, using model compounds to disentangle formulation-driven constraints and anatomical limitations.

The above observations advance our understanding of challenges faced in earlier studies with meloxicam-loaded microneedle patches.[10,30,32] Unlike meloxicam, which exhibited limited systemic absorption due to its low solubility (*i.e.*, 0.5 mg mL^{-1} in 1 : 1 DMSO : PBS) and moderate permeability,[33,34] both FITC-dextran and flunixin meglumine were measured at detectable systemic levels. FITC-dextran, with an average molecular weight of approximately 4 kDa (Sigma-Aldrich), was selected as a model hydrophilic fluorescent tracer due to its high-water solubility (*i.e.*, ≥30 mg mL^{-1}). Although no additional molecular weight verification was performed, the high plasma levels *in vivo* relative to the oral control supported the utility of FITC-dextran for assessing the performance of site-specific microneedle delivery systems.[35] In contrast, FLU exhibited moderate solubility (*i.e.*, 10 mg mL^{-1} in PBS, pH 7.2), and the comparatively lower systemic uptake was attributed to local tissue and anatomical factors at the application site, as described above.[36,37]

These findings not only highlight the role of drug physicochemical properties in transdermal delivery but also align with broader biological principles of molecular transport. For example, the intestinal epithelium in the gastrointestinal tract serves as a highly selective barrier that restricts the entry of large or hydrophilic molecules into systemic circulation.[38] This barrier function includes tight regulation of molecular size, permeability, and solute transport to the serosal side. Dextran, a high-molecular-weight carbohydrate, exemplifies such restricted permeability and is often employed as a biomarker in animal models to assess gut integrity and barrier disruption.[39] Therefore, the observed differences in systemic uptake between FITC-dextran, FLU, and meloxicam reinforce the need to consider solubility, permeability, molecular weight, and tissue-specific physiological barriers in the design and evaluation of transdermal drug delivery systems.[40–44]

Variations in skin lipid composition and subcutaneous fat thickness between swine and cattle have been proposed as contributing factors to differences in transdermal absorption, as lipophilic drugs must traverse the stratum corneum and diffuse through intercellular lipids before entering systemic circulation.[41,43] Swine typically exhibit greater backfat thickness (~1.8 cm) than cattle (~0.8–1.5 cm), which may result in drug sequestration in adipose tissue rather than effective systemic diffusion.[40,42] Dermal metabolism prior to systemic uptake has also been proposed as a limiting factor in the transdermal bioavailability of certain compounds, including FLU;[44] however, these mechanisms were not evaluated in this study. Recent studies have demonstrated the importance of evaluating dermal enzyme activity and drug stability at the application site to optimize systemic drug uptake by transdermal delivery systems, including microneedle patches.[45,46]

In summary, the pharmacokinetic data presented in Fig. 3 support the effectiveness of the microneedle patch drug delivery system and verify that FITC-dextran successfully reached systemic circulation. This outcome was best achieved when microneedle patches were applied to the neck, which served as a more favorable environment for transdermal drug absorption than the ear due to increased vascularization, thinner skin, better hydration, lower hair density, and enhanced lymphatic drainage.[25,28,47,48] These anatomical and physiological characteristics facilitate more efficient microneedle dissolution and drug diffusion into circulation. Future studies should further investigate these variables to optimize microneedle-based drug delivery for systemic applications.

The superior systemic absorption observed for FITC-dextran and FLU compared to meloxicam confirms that compound properties strongly influence transdermal delivery. As previously reported, meloxicam exhibited limited systemic absorption using the same microneedle platform.[10,49] The successful uptake of FITC-dextran and FLU in this study was attributed to the greater aqueous solubility and permeability of these compounds compared to meloxicam. While the microneedle formulation and application site play key roles, the physicochemical characteristics of the encapsulated drug remain decisive factors for achieving efficient systemic delivery. For example, certain drugs have stronger affinity with polymers used for drug delivery devices that may limit the rate of drug release.[50] Drug release from hydrophilic polymeric carriers often follows a combination of diffusion and swelling-controlled release described by the Higuchi or Korsmeyer–Peppas models.[51] Recent findings, including studies on polyvinyl alcohol/chitosan drug delivery scaffolds, highlighted that even weak or transient drug–matrix interactions, such as mucoadhesion and reversible binding, can modulate drug release rates.[52] Our previous findings with meloxicam highlight the fact that despite the use of hydrophilic polymers (PVA) to enhance drug solubility, the diffusion of meloxicam into the bloodstream was limited thus further confirming that the poor solubility of meloxicam plays a crucial role for its systemic absorption when delivered transdermally. Our findings here demonstrate that using more soluble compounds allow for greater drug diffusion and a systemic delivery.

The enhanced systemic absorption of FITC-dextran from microneedle patches applied to the neck suggests that future *in vivo* studies with microneedles loaded with meloxicam, FLU, or other NSAIDs should prioritize solubility enhancement strategies and explore alternative anatomical sites to improve bioavailability. Additional research is also needed to characterize microneedle dissolution rates *in vivo*, as current *in vitro* studies do not fully capture the complexities of microneedle–tissue interactions. A deeper understanding of microneedle dissolution kinetics under physiological conditions, taking into consideration constraints from anatomical limitations, will be essential for optimizing the microneedle patch for delivery of analgesics to pigs and other animals.

This work was designed as a pilot *in vivo* study to establish feasibility and identify trends in microneedle-mediated drug delivery for livestock applications. Accordingly, group sizes were small (n = 2–3), and results were analyzed descriptively (mean ± SD) rather than through formal statistical comparisons. Despite these constraints, the study successfully demonstrated systemic uptake of both FITC-dextran and FLU and revealed clear site-specific differences that inform future design. While FLU loaded microneedle patches were only tested on the ear in this study, the complementary FITC-dextran data highlighted the potential advantages of applying patches on the neck. Building on these findings, future studies will expand sample sizes and directly evaluate FLU delivery from the neck and other anatomical sites to more fully characterize systemic absorption and validate the promise of this novel drug delivery platform for pain management in livestock.

Conclusion

This study demonstrated the feasibility of using biodegradable microneedle patches for systemic drug delivery in livestock. The results highlighted the critical influence of anatomical site and drug physicochemical properties on transdermal absorption. Using FITC-dextran and FLU as model compounds, we confirmed that the optimized PVA–COL–CHI microneedle platform can achieve measurable systemic levels of hydrophilic and anti-inflammatory agents. These findings advance the broader understanding of microneedle-mediated pharmacokinetics in veterinary species. Future efforts are needed to measure *in situ* dissolution kinetics, identify solubility-enhancing formulations, and extend pharmacokinetic profiling to guide dose optimization. Overall, the findings of this study support the continued development of practical, stress-free, microneedle-based analgesic and therapeutic systems that improve animal welfare and enable sustainable livestock management.

Author contributions

Katherine A. Miranda-Muñoz: Methodology, writing – original draft preparation, visualization, formal analysis, data curation, investigation. Tsungcheng Tsai: Conceptualization, resources, *in vivo* data curation, *in vivo* data analysis, writing reviewing and editing, and investigation. Jacy L. Riddle: Data curation, investigation, and data analysis. Ke He & Lee Blaney: Conceptualization, resources, data curation, data analysis, writing – review and editing. Jeremy G. Powell & Jorge Almodovar: Conceptualization, supervision, writing reviewing and editing, resources, funding acquisition, project administration.

Conflicts of interest

The authors declare no conflicts of interest.

Data availability

The authors confirm that the data supporting the findings of this study are available within the article.

Supplementary information (SI) is available. Supplementary files contain raw fluorescent data and LC-MS/MS from plasma samples. See DOI: https://doi.org/10.1039/d5pm00203f.

Acknowledgements

This work was financially supported by the United States Department of Agriculture (award no. 2021-67015-35675). The authors thank Dr Mourad Benamara from the University of Arkansas for SEM access.

References

1 J. N. Fernandes, P. H. Hemsworth, G. J. Coleman and A. J. Tilbrook, Costs and benefits of improving farm animal welfare, *Agriculture*, 2021, **11**(2), DOI: 10.3390/agriculture11020104.

2 A. Balzani and A. Hanlon, Factors that influence farmers' views on farm animal welfare: A semi-systematic review and thematic analysis, *Animals*, 2020, **10**(9), DOI: 10.3390/ani10091524.

3 J. Lakritz, Veterinary regulatory concerns associated with anesthesia and analgesia for food animals, in *Pharmacology in Veterinary Anesthesia and Analgesia*, ed. T. Aarnes and P. Lerche, Wiley, Hoboken (NJ), 1st edn, 2024, pp. 31–35. DOI: 10.1002/9781118975169.ch$_3$.

4 T. Beyene, Veterinary drug residues in food-animal products: Its risk factors and potential effects on public health, *J. Vet. Sci. Technol.*, 2015, **7**(1), 1–7, DOI: 10.4172/2157-7579.1000285.

5 Vets Craft, Route of drug administration in animals [Internet]. 2022 Feb 5 [cited 2025 Jul 21]. Available from: https://www.vetscraft.com/route-of-drug-administration-in-animals/.

6 P. T. Reeves, C. Roesch and M. Nic Raghnaill, How drugs are given in animals [Internet]. Merck Veterinary Manual. 2011 Jul [updated 2024 Sep; cited 2025 Jul 21]. Available from: https://www.merckvetmanual.com/special-pet-topics/drugs-and-vaccines/how-drugs-are-given-in-animals.

7 Y. Hao, W. Li, X. L. Zhou, F. Yang and Z. Y. Qian, Microneedles-based transdermal drug delivery systems: A review, *J. Biomed. Nanotechnol.*, 2017, **13**(12), 1581–1597, DOI: 10.1166/jbn.2017.2474.

8 H. X. Nguyen, Beyond the needle: Innovative microneedle-based transdermal vaccination, *Medicines*, 2025, **12**(1), DOI: 10.3390/medicines12010004.

9 R. Samineni, J. Chimakurthy and S. Konidala, Emerging role of biopharmaceutical classification and biopharmaceutical drug disposition system in dosage form development: A systematic review, *Turk. J. Pharm. Sci.*, 2022, **19**(6), 706–713, DOI: 10.4274/tjps.galenos.2021.73554.

10 K. Miranda-Muñoz, K. Midkiff, A. Woessner, M. Afshar-Mohajer, M. Zou, E. Pollock, D. Gonzalez-Nino, G. Prinz, L. Hutchinson, R. Li, K. Kompalage, C. T. Culbertson, R. J. Tucker, H. Coetzee, T. Tsai, J. Powell and J. Almodovar, A multicomponent microneedle patch for the delivery of meloxicam for veterinary applications, *ACS Nano*, 2024, **18**(37), 25716–25739, DOI: 10.1021/acsnano.4c08072.

11 S. Berg, D. Suljovic, L. Kärrberg, M. Englund, H. Bönisch, I. Karlberg, N. Van Zuydam, B. Abrahamsson, A. M. Hugerth, N. Davies and C. A. S. Bergström, Intestinal absorption of FITC-dextrans and macromolecular model drugs in the rat intestinal instillation model, *Mol. Pharm.*, 2022, **19**(7), 2564–2572, DOI: 10.1021/acs.molpharmaceut.2c00261.

12 G. Y. Ahn, H. S. Eo, D. Kim and S. W. Choi, Transdermal delivery of FITC-dextrans with different molecular weights using radiofrequency microporation, *Biomat. Res.*, 2020, **24**(1), 1–7, DOI: 10.1186/s40824-020-00201-7.

13 N. Barbero, C. Barolo and G. Viscardi, Bovine serum albumin bioconjugation with FITC, *World J. Chem. Educ.*, 2016, **4**(4), 93–96.

14 Sigma-Aldrich. Fluorescein isothiocyanate–dextran [Internet]. [cited 2025 Jul 21]. Available from: https://www.sigmaaldrich.com/US/en/technical-documents/technical-article/cell-culture-and-cell-culture-analysis/cell-based-assays/fluorescein-isothiocyanate-dextran.

15 F. P. Gobbi, P. A. Di Filippo, L. D. M. Mello, *et al.*, Effects of flunixin meglumine, firocoxib, and meloxicam in equines after castration, *J. Equine Vet. Sci.*, 2020, **94**, 103229, DOI: 10.1016/j.jevs.2020.103229.

16 J. L. Davis, Pharmacologic principles, in *Equine Internal Medicine*, ed. S. M. Reed, W. M. Bayly and D. C. Sellon, Elsevier, St. Louis (MO), 4th edn, 2018, pp. 79–137. DOI: 10.1016/B978-0-323-44329-6.00002-4.

17 J. L. Buur, R. E. Baynes, G. Smith and J. E. Riviere, Pharmacokinetics of flunixin meglumine in swine after intravenous dosing, *J. Vet. Pharmacol. Ther.*, 2006, **29**(5), 437–440, DOI: 10.1111/j.1365-2885.2006.00788.x.

18 P. L. Toutain, A. Autefage, C. Legrand and M. Alvinerie, Plasma concentrations and therapeutic efficacy of phenylbutazone and flunixin meglumine in the horse: pharmacokinetic/pharmacodynamic modelling, *J. Vet. Pharmacol. Ther.*, 1994, **17**(6), 459–469, DOI: 10.1111/j.1365-2885.1994.tb00278.x.

19 K. He, A. Timm and L. Blaney, Simultaneous determination of UV-filters and estrogens in aquatic invertebrates by modified quick, easy, cheap, effective, rugged, and safe extraction and liquid chromatography tandem mass spectrometry, *J. Chromatogr. A*, 2017, **1509**, 91–101, DOI: 10.1016/j.chroma.2017.06.039.

20 A. M. Kocot, E. Jarocka-Cyrta and N. Drabińska, Overview of the importance of biotics in gut barrier integrity, *Int. J. Mol. Sci.*, 2022, **23**(6), 3202, DOI: 10.3390/ijms23063202.

21 J. P. Gleeson, K. C. Fein, N. Chaudhary, R. Doerfler, A. N. Newby and K. A. Whitehead, The enhanced intestinal permeability of infant mice enables oral protein and macromolecular absorption without delivery technology, *Int. J. Pharm.*, 2021, **593**, 120148, DOI: 10.1016/j.ijpharm.2020.120148.
22 J. Liu, P. Y. Teng, W. K. Kim and T. J. Applegate, Assay considerations for fluorescein isothiocyanate-dextran (FITC-d): an indicator of intestinal permeability in broiler chickens, *Poult. Sci.*, 2021, **100**(2), 100929, DOI: 10.1016/j.psj.2020.12.030.
23 Z. Zhang and W. Tang, Drug metabolism in drug discovery and development, *Acta Pharm. Sin. B*, 2018, **8**(5), 721–732, DOI: 10.1016/j.apsb.2018.04.003.
24 S. T. Susa and V. H. A. Ch, Drug metabolism, in *StatPearls*, StatPearls Publishing, Treasure Island (FL), 2023. Available from: https://www.ncbi.nlm.nih.gov/books/NBK442023/.
25 P. C. Mills and S. E. Cross, Transdermal drug delivery: Basic principles for the veterinarian, *Vet. J.*, 2006, **172**(2), 218–233, DOI: 10.1016/j.tvjl.2005.09.006.
26 A. Z. Garza, S. B. Park and R. Kocz, Drug elimination, in *StatPearls*, StatPearls Publishing, Treasure Island (FL), 2023. Available from: https://www.ncbi.nlm.nih.gov/books/NBK547662/.
27 S. L. Marks and J. Taboada, Transdermal therapeutics, *J. Am. Anim. Hosp. Assoc.*, 2003, **39**(1), 19–21, DOI: 10.5326/0390019.
28 I. Singh and A. Morris, Performance of transdermal therapeutic systems: effects of biological factors, *Int. J. Pharm. Invest.*, 2011, **1**(1), 4–9, DOI: 10.4103/2230-973X.76721.
29 H. Kathuria, D. Lim, J. Cai, B. G. Chung and L. Kang, Microneedles with tunable dissolution rate, *ACS Biomater. Sci. Eng.*, 2020, **6**(9), 4905–4914, DOI: 10.1021/acsbiomaterials.0c00759.
30 S. L. Marks, Where are we with transdermal drug administration? [Internet]. Veterinary Information Network; 2003 [cited 2025 Jul 21]. Available from: https://www.vin.com/apputil/project/defaultadv1.aspx?pid=11154&catid=&id=3847278.
31 M. D. Pairis-Garcia, L. A. Karriker, A. K. Johnson, B. Kukanich, L. Wulf, S. Sander, *et al.*, Pharmacokinetics of flunixin meglumine in mature swine after intravenous, intramuscular, and oral administration, *BMC Vet. Res.*, 2013, **9**, 165, DOI: 10.1186/1746-6148-9-165.
32 H. C. Kittrell, J. P. Mochel, J. T. Brown, *et al.*, Pharmacokinetics of intravenous, intramuscular, oral, and transdermal administration of flunixin meglumine in preweaned piglets, *Front. Vet. Sci.*, 2020, **7**, 586, DOI: 10.3389/fvets.2020.00586.
33 P. Luger, K. Daneck, W. Engel, G. Trummlitz and K. Wagner, Structure and physicochemical properties of meloxicam, a new NSAID, *Eur. J. Pharm. Sci.*, 1996, **4**(3), 175–187, DOI: 10.1016/S0928-0987(96)00462-1.
34 Cayman Chemical, Meloxicam product information sheet, item no. 14906 [Internet]. Published 2022 Nov 8 [cited 2025 Jul 21]. Available from: https://cdn.caymanchem.com/cdn/insert/14906.pdf.
35 Sigma-Aldrich. Fluorescently labeled dextran [Internet]. [cited 2025 Jul 21]. Available from: https://www.sigmaaldrich.com/US/en/technical-documents/technical-article/cell-culture-and-cell-culture-analysis/imaging-analysis-and-live-cell-imaging/fluorescently-labeled-dextrane.
36 Cayman Chemical, Flunixin (meglumine) product information sheet, item no. 26644 [Internet]. Published 2022 Dec 19 [cited 2025 Jul 21]. Available from: https://cdn.caymanchem.com/cdn/insert/26644.pdf.
37 United States Pharmacopeial Convention. Flunixin (veterinary—systemic) [Internet]. Published 2007 [cited 2025 Jul 21]. Available from: https://cdn.ymaws.com/www.aavpt.org/resource/resmgr/imported/flunixin.pdf.
38 K. R. Groschwitz and S. P. Hogan, Intestinal barrier function: molecular regulation and disease pathogenesis, *J. Allergy Clin. Immunol.*, 2009, **124**(1), 3–20, DOI: 10.1016/j.jaci.2009.05.038.
39 V. A. Kuttappan, E. A. Vicuña, J. D. Latorre, *et al.*, Evaluation of gastrointestinal leakage in multiple enteric inflammation models in chickens, *Front. Vet. Sci.*, 2015, **2**, 66, DOI: 10.3389/fvets.2015.00066.
40 C. Ohnishi and M. Satoh, Estimation of genetic parameters for performance and body measurement traits in Duroc pigs selected for average daily gain, loin muscle area, and backfat thickness, *Livest. Sci.*, 2018, **214**, 161–166, DOI: 10.1016/j.livsci.2018.05.022.
41 M. R. Prausnitz and R. Langer, Transdermal drug delivery, *Nat. Biotechnol.*, 2008, **26**(11), 1261–1268, DOI: 10.1038/nbt.1504.
42 U. J. Schröder and R. Staufenbiel, Invited review: methods to determine body fat reserves in the dairy cow with special regard to ultrasonographic measurement of backfat thickness, *J. Dairy Sci.*, 2006, **89**(1), 1–14, DOI: 10.3168/jds.S0022-0302(06)72064-1.
43 J. D. Wood, M. Enser, A. V. Fisher, *et al.*, Fat deposition, fatty acid composition and meat quality: a review, *Meat Sci.*, 2008, **78**(4), 343–358, DOI: 10.1016/j.meatsci.2007.07.019.
44 P. L. Toutain and A. Bousquet-Mélou, Bioavailability and its assessment, *J. Vet. Pharmacol. Ther.*, 2004, **27**(6), 455–466, DOI: 10.1111/j.1365-2885.2004.00604.x.
45 N. Lau, K. Phan and Y. Mohammed, Role of skin enzymes in metabolism of topical drugs, *Metab. Target Organ Damage*, 2024, **4**(4), 17, DOI: 10.20517/mtod.2024.17.
46 I. Batool, N. Zafar, Z. Ahmad, A. Mahmood, R. M. Sarfraz, S. Shchinar, *et al.*, Nanoparticle-loaded microneedle patch for transdermal delivery of letrozole, *Bionanoscience*, 2024, **14**(3), 2131–2144, DOI: 10.1007/s12668-024-01257-1.
47 A. Summerfield, F. Meurens and M. E. Ricklin, The immunology of the porcine skin and its value as a model for human skin, *Mol. Immunol.*, 2015, **66**(1), 14–21, DOI: 10.1016/j.molimm.2014.10.023.
48 C. Uhm, H. Jeong, S. H. Lee, J. S. Hwang, K. M. Lim and K. T. Nam, Comparison of structural characteristics and molecular markers of rabbit skin, pig skin, and recon-

structed human epidermis for an ex vivo human skin model, *Toxicol. Res.*, 2023, **39**(3), 477–484, DOI: 10.1007/s43188-023-00185-1.

49 D. A. Castilla-Casadiego, K. A. Miranda-Muñoz, J. L. Roberts, A. D. Crowell, D. Gonzalez-Niño, D. Choudhury, *et al.*, Biodegradable microneedle patch for delivery of meloxicam for managing pain in cattle, *PLoS One*, 2022, **17**(8), e0272784, DOI: 10.1371/journal.pone.0272784.

50 M. S. Jose and S. Sumathi, A review of electrospun polymeric fibers as potential drug delivery systems for tunable release kinetics, *J. Sci.:Adv. Mater. Devices*, 2025, **10**(3), 100933, DOI: 10.1016/j.jsamd.2025.100933.

51 Y. Fu and W. J. Kao, Drug release kinetics and transport mechanisms of non-degradable and degradable polymeric delivery systems, *Expert Opin. Drug Delivery*, 2010, **7**(4), 429–444, DOI: 10.1517/17425241003602259.

52 K. G. Nathan, K. Genasan and T. Kamarul, Polyvinyl alcohol-chitosan scaffold for tissue engineering and regenerative medicine application: a review, *Mar. Drugs*, 2023, **21**(5), 273, DOI: 10.3390/md21050273.